*Korean J. Chem. Eng.*, 37(7), 1266-1273 (2020)
DOI: 10.1007/s11814-020-0545-y

pISSN: 0256-1115
eISSN: 1975-7220

# Surface morphologies and wetting properties of layer-by-layer assembled films of polyelectrolytes with bimodal molecular weight distribution

**Choonghyun Sung†, Subin Choi, and Jinkyeong Kim**

Polymeric Materials Engineering Major, Dong-eui University, 176 Eomgwang-ro, Busanjin-gu, Busan 47340, Korea
(*Received 31 January 2020 • Revised 7 March 2020 • Accepted 16 March 2020*)

**Abstract**−Layer-by-layer (LbL) assembly has been rigorously applied to the construction of superhydrophobic surfaces. Typically, this involves generating a hierarchical porous structure which is then coated with a low surface energy compound. In this study, a porous LbL film was constructed from poly(allylamine hydrochloride) (PAH)/poly(acrylic acid) (PAA) using a PAA solution with a bimodal molecular weight distribution. This solution was prepared by mixing two PAA solutions with different average molecular weights (100,000 and 15,000 g/mol). The mixing ratio was adjusted for fine control of the porous structure, which was induced by acid treatment at pH 2.0-2.4. Generally, surface pore structure was weakened as the 15,000 g/mol PAA ratio increased. However, the surface roughness decreased or increased as the 15,000 g/mol PAA ratio increased depending on the acid treatment pH and time. The porous LbL films were coated with fluorinated silane to make them hydrophobic. When the acid condition was pH 2.4 for 5 min, the water contact angle decreased significantly from 132° to minimum of 105° as the amount of 15,000 g/mol PAA increased. However, at pH 2.0 for 5 min, the water contact angle decreased smaller from 148° to 139° as the amount of 15,000 g/mol PAA increased.

Keywords: Layer-by-layer, Porous, Superhydrophobic, Molecular Weight, Multilayer

## INTRODUCTION

There has been significant interest in systematic control of the wetting properties of surfaces due to the wide range of applications. Superwetting surfaces such as superhydrophilic, superhydrophobic, superoleophobic, and liquid-infused slippery surfaces have been extensively studied for a variety of applications such as antifogging [1], self-cleaning [2], drag reduction [3], anti-icing [4], anti-corrosion [5], and oil/water separation [6]. There are numerous excellent reviews concerning superwetting surfaces [7-10].

A surface is superhydrophobic if it exhibits a water contact angle greater than 150° with contact angle hysteresis below 5° or 10°. The discovery that superhydrophobicity of lotus is accomplished by micro and nanoscale hierarchical structure with low surface energy leading to extensive research into the synthesis of superhydrophobic surface. Various techniques such as etching [11], anodization [12], electrochemical deposition [13], sol-gel [14], hydrothermal reaction [15], and electrospinning [16] have been employed to produce hierarchical structures. However, many of these approaches are rather expensive, difficult to scale up, or require harsh chemical environments.

LbL assembly technique has been recognized as a simple and versatile way to fabricate superwetting coatings [17-21]. Nanoscale multilayer films are constructed through electrostatic interaction, hydrogen bonding, and covalent bonding. Adjusting the assembly, post-assembly condition along with a wide selection of material allows the surface chemistry and topography to be controlled at a molecular level. Furthermore, LbL assembly is suitable for an aqueous based processing and it is a conformal coating method that can be used to coat any shape of substrate.

Superhydrophobic surface has been fabricated by constructing hierarchical surface which is then coated with a low surface energy compound. The majority of research has concentrated on preparing proper hierarchical structure, and fluorinated or alkyl silanes are typically used for low surface energy compounds. Several approaches have been used to fabricate superhydrophobic coatings using LbL assembly technique. The most popular method incorporates nanoparticles in the LbL film for hierarchical structure. Silica, graphene, carbon nanotube, metal oxide, and wax nanoparticles or nanomaterials have been used extensively. LbL films of polymer/nanoparticle and nanoparticle-only have been reported. Shiratori et al. prepared nanoparticle-only superhydrophobic surface via calcination of polylectrolyte/nanoparticle LbL film [22]. Guo et al. produced electrically conductive superhydrophobic fabric by coating PET fiber with LbL film made from carbon nanotube and polyelectrolyte which was then coated with polydimethylsiloxane [23]. In addition, a transparent superwetting LbL film with enhanced durability has been prepared using polyelectrolyte and fluorinated silsesquioxane nanoparticles [24].

Another approach involves fabricating the film without nanoparticles. One such method involves constructing an LbL film using polymer/polymer or polymer/surfactant complex [25,26]. These complexes aggregate on the LbL film to form a very rough surface. A superhydrophobic surface has also been prepared by fluorinating hierarchical surface obtained from exponential growth of polyelectrolyte multilayer [27-29]. Alternatively, a porous structure has been used to fabricate hierarchical topography. Although there are

†To whom correspondence should be addressed.
E-mail: chsung@deu.ac.kr

some reports that porous structure is formed during reactive LbL assembly of azlactone functionalized polymers [30,31], most porous LbL films have been constructed by post-assembly treatment. Exposing a weak polyelectrolyte system such as poly(allylamine hydrochloride) (PAH)/poly(acrylic acid) (PAA) [32-34] or poly(ethylene imine)/PAA [35,36] to acidic or basic solution results in micro- or nanoscale pores depending on assembly and post acid treatment condition. The proposed mechanism underlying pore formation is as follows [37]. When immersed in acid, an LbL film swells as protonation of the acid group causes breakage of the ionic crosslinks. Subsequent immersion in neutral water cause the film to contract as the ionic crosslinks reform and micro- or nanoscale water pockets are created. When the film is dried, porous structure is obtained.

Rubner et al. were the first to employ porous PAH/PAA LbL film to prepare stable superhydrophobic coating [38]. First, a honeycomb like multilayer surface was prepared by 6 h two-stage post acid treatment. Then, silica nanoparticles were deposited, and finally, it was treated with fluorinated silane. Zacharia et al. also applied two-staged post acid treatment of branched poly(ethylene imine)/PAA LbL film to prepare porous hierarchical structure [27]. These films were used for liquid-infused slippery surface with additional deposition of silica nanoparticles. Recently, Lee et al. prepared superhydrophobic surface by fluorinating synchronously generated nano- and microscale hierarchical porous PAH/PAA multilayer without the use of nanoparticles [39]. It is desirable to avoid additional deposition of nanoparticle because it makes the fabrication process more complex and time-consuming. They showed that an appropriate acid treatment condition and PAH/PAA molecular weights are critical for the synchronous generation of nano- and microscale hierarchical structure.

Inspired by the superhydrophobic surface prepared by using hierarchical porous PAH/PAA without nanoparticles, this study investigated porous multilayer using a PAA solution with bimodal molecular weight (MW) distribution. Pore sizes of 0.3-2 μm have been reported when PAA of relatively high molecular weight of ~100,000 g/mol was used in PAH/PAA LbL assembly [32,33]. However, it has been shown that large pores in excess of 5 μm are formed when PAA with a low MW of 1,000-10,000 g/mol [40,41]. In this work, bimodal MW PAA solution was prepared by mixing two PAA solutions with average MWs of 100,000 and 15,000 g/mol in order to achieve fine control of the porous structure. The surface morphologies of acid-treated porous LbL films were explored and the water contact angles of fluorinated porous LbL films were investigated. The aim is to show that it is possible to control the surface morphology and water contact angle of LbL films by controlling the post acid treatment pH and time as well as the PAA mixing ratio. To our knowledge, this is the first report of a porous LbL film being produced using polyelectrolyte with a bimodal MW distribution.

## EXPERIMENTAL

### 1. Materials

Poly(allylamine hydrochloride) (PAH) (160,000 g/mol) was purchased from Alfa Aesar. Poly(acrylic acid) (PAA) (100,000 g/mol (100K) and 15,000 g/mol (15K)) and Trichloro(1H,1H,2H,2H-perfluorooctyl silane) (TCPFS) were obtained from Aldrich. All the polymer solutions were prepared at the concentration of 10 mM based on the molar mass of the repeat unit by dissolving the polymers in deionized water. The pH values of the solutions were adjusted using HCl or NaOH.

### 2. Fabrication of LbL Film

LbL films were coated on slide glasses using a programmable multiple dip-coater (HT-17, Hantech). The slide glasses were cleaned by sonicating in acetone, methanol, and water for 10 min each. They were then dried in an oven at 80 °C and oxygen plasma-treated for 10 min immediately before LbL assembly using plasma cleaner (Harrick, 32G). For the LbL assembly, the slide glasses were immersed in PAH solution (pH 7.5) for 15 min and then rinsed in a water bath three times for 2, 1, and 1 min each. Next, they were immersed in PAA solution (pH 3.5) for 15 min and then rinsed in a water bath as before. This process was repeated to yield 20.5 bilayers of $(PAH/PAA)_{20}PAH$. The samples were dried in an oven at 80 °C for 15 min. PAA solution was prepared by mixing 100K and 15K PAA solution at five volume ratios: 100 : 0, 75 : 25, 50 : 50, 25 : 75, and 0 : 100.

### 3. Post Acid Treatment and Hydrophobic Treatment

The as-prepared PAH/PAA LbL films were exposed to acidic solution of pH 2.0-2.4 for 5 min or 1 h, and then rinsed with deionized water for 2 min. Next, the samples were dried in convection oven at 80 °C for 15 min, then heated at 180 °C for 2 h to crosslink porous structure [20,38]. Then, TCPFS was deposited on the surface of the crosslinked samples through chemical vapor deposition under atmospheric conditions. The films were put into a 150 ml sealed bottle containing 90 μL of TCPFS, and the bottle was left for 6 h at room temperature [42,43].

### 4. Characterization

The thickness and root mean square surface roughness was measured using a profilometer (Alphastep D-100, KLA-Tencor). Scanning electron microscopy (SEM) images of surface morphologies of acid-treated samples were obtained using Quanta 600 microscope (Hitachi) at an accelerating voltage of 15 kV. An 8 nm thick layer of Pt was sputtered onto the film to suppress charging. Water contact angles were measured by drop shape analysis of 4 μL water droplet dispensed on the film at five different positions using Pheonix-150 (SEO).

## RESULTS AND DISCUSSION

The thickness and roughness of LbL films were measured prior to post acid treatment (Fig. 1). As 15K PAA ratio increased from 0% to 75% (i.e., 100K PAA decreased from 100% to 25%), the film thickness increased from 1,087 to 2,000 nm. As for the roughness, when the solution was 100% 100K PAA, the roughness was approximately 50 nm. However, as the 15K PAA ratio rose above 50%, the roughness decreased to 10 nm. These results suggest that the PAA composition of the LbL film changed according to the mixing ratio of solution. Porous structure was not observed prior to acid treatment. The increase in film thickness and decrease in roughness with the increase in the amount of 15K PAA was attributed to faster adsorption and less coiled chain conformation of 15K PAA compared to 100K PAA [44]. At assembly pH of 3.5, the degree of ionization of PAA is low and electrostatic interaction between PAA

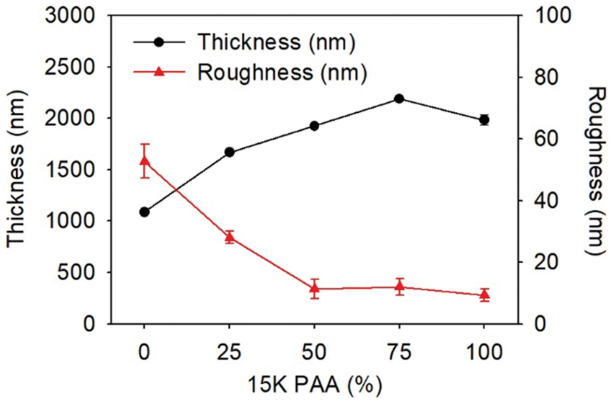


**Fig. 1. Thickness and roughness of the as-made LbL films.**

and PAH on the film surface is relatively weak. Therefore, as the MW of PAA increases, the adsorption of PAA onto the film surface is slowed due to the poor chain mobility, which results in slow film growth. In addition, more coiled conformation due to the higher MW of PAA coupled with ionization results in high surface roughness.

The as-made LbL films were immersed in acidic solution to generate the porous structure. The effects of 100K/15K PAA ratio and acid treatment pH on the surface morphologies of the acid-treated LbL films were examined. For acid treatment time, 5 min and 1 h were selected. According to the previous studies, time less than 5 min was frequently used to generate small nano- or micro-pores, and time longer than 1 h was used to generate larger pores or hierarchical structure. Fig. 2 shows the SEMS images of acid-treated LbL films at varying pH for 5 min. When the films prepared using 100% 100K PAA (1st column) were treated at pH 2.4, pores with diameter of 0.5-3 μm were observed. However, when pH decreased to 2.2 or 2.0, crater-like pores of ~5 μm were observed.

Next, we examined the effect of increasing 15K PAA ratio on the surface morphology at each pH (rows in Fig. 2). At pH 2.4, the pores became smaller and surface became smoother as the amount of 15K PAA increased until 75%. At 100% 15K PAA, it was difficult to see clear pores. At pH values of 2.2 and 2.0, increasing the amount of 15K PAA had a similar effect. However, for 15K PAA ratios of 25%, 50%, and 75%, the pores in the films treated at pH 2.2 were more distinct and clear than those treated at pH 2.4. At pH 2.0, crater-like pores were observed until the 15K PAA ratio reached 25%, but distinct pores were not observed once the ratio exceeded 50%. Overall, when 100% 15K PAA was used, a clear porous structure was not observed.

The surface morphology of LbL films was also examined when the acid treatment time was increased to 1 h (Fig. 3). Overall, the pore size increased compared to the films treated for 5 min. At pH 2.4 and 2.2, the pores were between 300 nm and 5 μm in diameter, regardless of 15K PAA ratio. This was in contrast to the results for an acid treatment of 5 min where pore size decreased as the 15K PAA ratio increased. However, at pH 2.0, smaller pores of 100-500 nm were observed in all the films except those assembled with 100% 100K PAA. For the films treated at pH 2.0 for 5 min, these small pores were hardly visible.

The roughness of acid-treated samples was measured with a profilometer (Fig. 4). At pH 2.4 and a treatment time of 5 min, roughness decreased from 311 nm to minimum of 116 nm as the 15K PAA ratio increased. When the treatment time was increased to 1 h, the roughness decreased from 383 nm to 300 nm as the 15K PAA ratio increased. Overall, the films treated for 1 h showed greater roughness than those treated for 5 min. At pH 2.2, roughness was highly influenced by both the 15K PAA ratio and acid treatment time. When the acid treatment time was 5 min, roughness decreased from 462 nm to 173 nm as the 15K PAA ratio increased. However, when the treatment time was 1 h, roughness in-

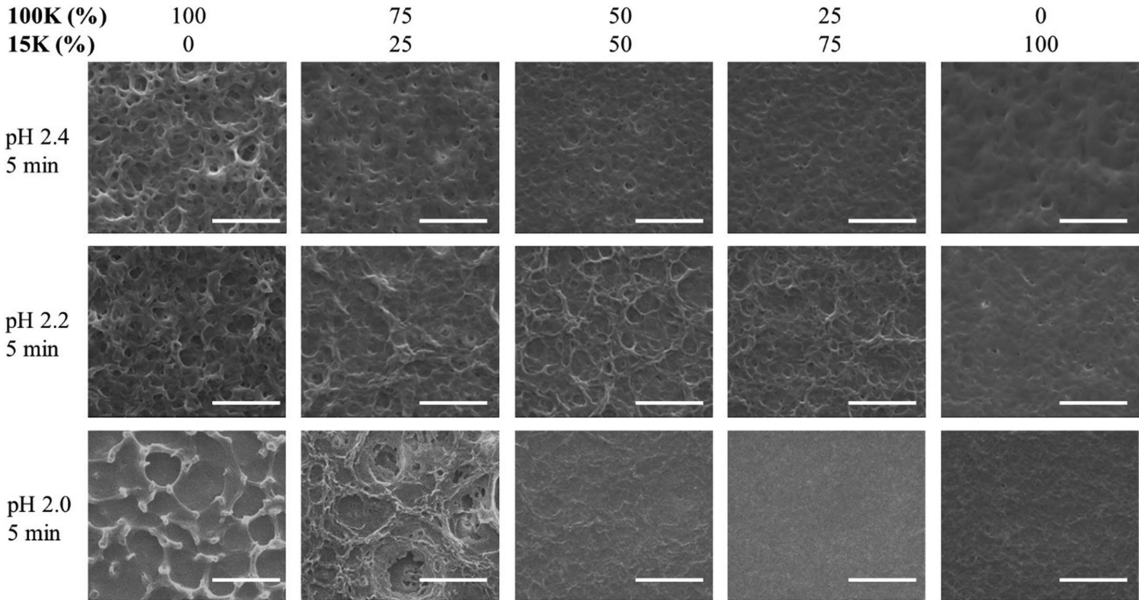


**Fig. 2. SEM images of acid-treated LbL film at different pH and 15K PAA ratio with an acid treatment time of 5 min. The scale bar for all the images is 10 μm.**

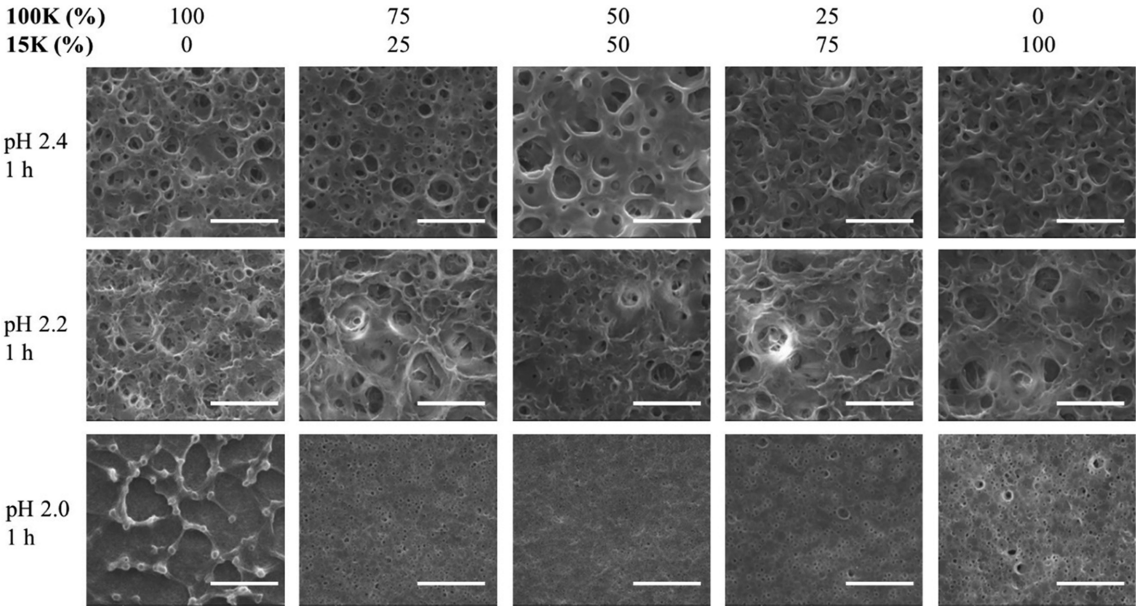


**Fig. 3. SEM images of acid-treated LbL films at different pH values and 15K PAA ratios with an acid treatment time of 1 h. The scale bar for all the images is 10 μm.**

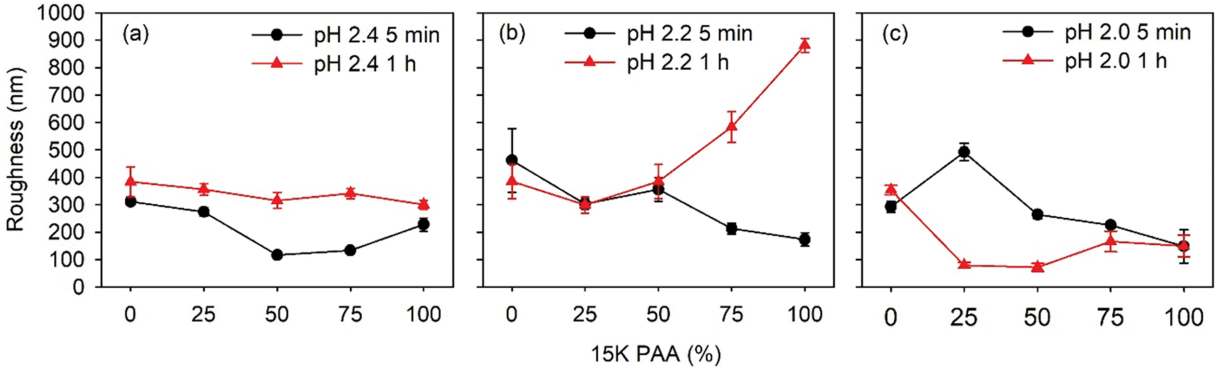


**Fig. 4. Roughness of PAH/PAA LbL film treated at (a) pH 2.4, (b) pH 2.2, and (c) pH 2.0. The same scale of roughness applies to all the figures.**

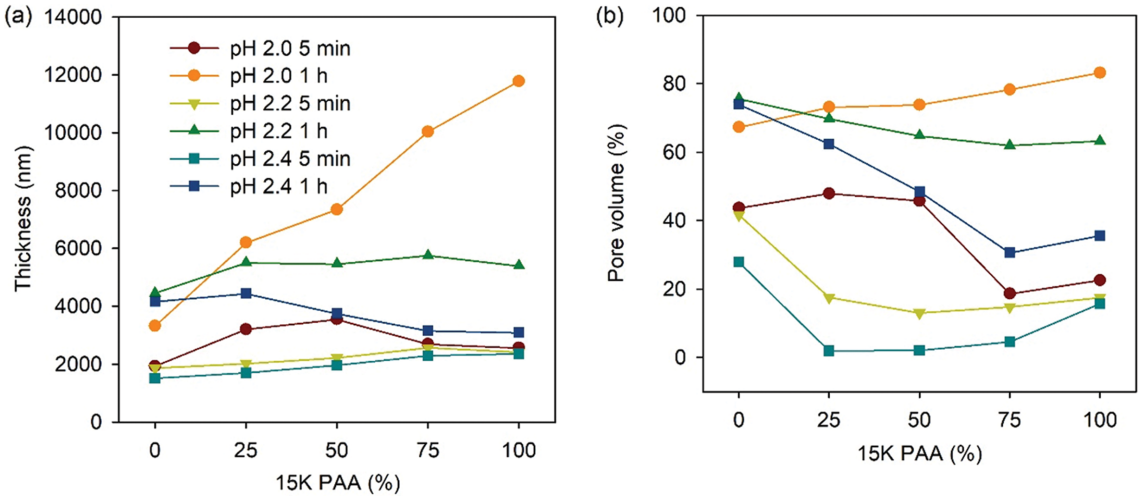


**Fig. 5. (a) Film thickness and (b) pore volume of the acid-treated PAH/PAA LbL film. The legend applies to both figures.**

creased significantly from 385 nm to 880 nm as the 15K PAA ratio increased. In contrast, at pH 2.0 the roughness decreased when treatment time was increased from 5 min to 1 h for the 15K PAA ratios between 25% and 75%, contrary to the observation for pH 2.4. Overall, the effect of 15K PAA ratio, pH, and treatment time on roughness is fairly consistent with the surface topography observed in SEM images.

The thickness of acid-treated film was measured (Fig. 5(a)). In general, film thickness increased as the acid treatment time increased from 5 min to 1 h. At 5 min, the film thickness did not change much as the 15K PAA ratio increased. Furthermore, pH did not have a significant effect on the film thickness, although thickness was a little higher at pH 2.0 than pH 2.4 and 2.2 when the 15K PAA ratio was 25% or 50%. However, if acid treatment time increased to 1 h, the pH and 15K PAA ratio both had a great effect on the film thickness. In particular, at pH 2.0, film thickness increased from 2,300 nm to 11,800 nm as the 15K PAA ratio increased from 0% to 100%.

Using the thickness data of the as-made (Fig. 1) and acid-treated (Fig. 5(a)) films, pore volume (%) was calculated using the following equation [38].

$$\text{Pore volume (\%)} = \frac{(\text{thickness after acid treatment} - \text{thickness before acid treatment})}{\text{thickness after acid treatment}} \times 100$$

The pore volume (%) was presented as a function of acid treatment pH and the 15K PAA ratio (Fig. 5(b)). As a whole, at a given 15K PAA ratio, the films treated for 1 h had a higher pore volume than those treated for 5 min, regardless of pH. Furthermore, for a given acid treatment time, 5 min or 1 h, pore volume increased as the acid treatment pH increased. For example, when the 15K PAA ratio was 75% and treatment time was 1 h, pore volumes were 30%, 63%, and 80% when the pH was 2.4, 2.2, and 2.0, respectively.

The effect of PAA mixing ratio on the pore volume at acid treatment time of 1 h is of particular interest. When 100% 100K PAA was used, pore volume was 67-76%, which was not greatly influenced by acid treatment pH. However, as the 15K PAA (%) increased, pore volume became highly dependent on the pH. At pH 2.4, pore volume decreased from 74% to 35% as the 15K PAA ratio increased. At pH 2.2, pore volume decreased slightly from 76% to 62%. In contrast, at pH 2.0, pore volume (%) increased from 67% to 85%. Therefore, at 100% 15K PAA, pore volume varied between 35% to 85% depending on the acid treatment pH, contrary to the small variation in pore volume when 100% of 100K PAA was used.

The pH dependence of pore volume according to PAA mixing ratio was verified using the cross-sectional images of acid-treated samples (Fig. 6). For both samples prepared using both 100% 100K and 100% 15K PAAs, pore structure could not be effectively identified when treated at pH 2.4 for 5 min. However, when the acid treatment time was increased to 1 h, a difference in the pore structure was detected. For the samples prepared using 100% 100K PAA, pores with 1-5 μm in diameter were clearly visible for both pH 2.4 and 2.0. However, for the samples prepared using 15K PAA, pore structure depended on acid treatment pH. At pH 2.4, pores were collapsed rather than spherical and pore volume was relatively small. On the other hand, at pH 2.0, pores ranged from 1-2.5 μm, and antisymmetric pore structure with smaller pores near the substrate and larger pores near the film surface was observed. These cross-sectional images are consistent with the pore volumes calculated from the change in film thickness.

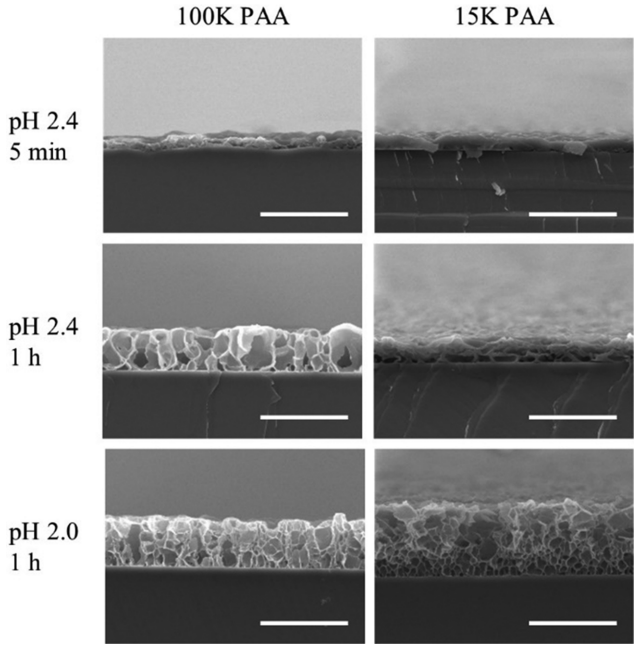


**Fig. 6. SEM images of cross-section of PAH/PAA LbL films treated at varying pH and time. The scale bar is 10 μm.**

To make a hydrophobic surface, porous LbL films were coated with fluorinated silane, TCPFS, and water contact angle (WCA) was then measured (Fig. 7). At pH 2.4, the WCA generally decreased as the 15K PAA ratio increased (Fig. 7(a)). At the treatment time of 5 min, the WCA decreased from 132° to 105-116° as the 15K PAA ratio increased. At a treatment time of 1 h, the WCA decreased from 143° to a minimum 117-128° as the 15K PAA ratio increased. As noted in Figs. 3, 4 and 5, roughness and pore volume decreased a little, and the surface texture was weakened as the 15K PAA ratio increased at the pH 2.4 condition. Thus, the decrease in WCA with the increase in 15K PAA ratio is likely due to weakening of porous structure and decrease of roughness rather than pore volume effect. Another possibility is stability of contact angle. We found that WCA decreased with measurement time when 100% 15K PAA was used in LbL assembly, while WCA was fairly constant when 100% 100K PAA was used. It is associated with the facile penetration of water droplet or reorganization of polymer chains on the surface due to the 15K PAA. This will be discussed later in Fig. 8. Furthermore, at a given 15K PAA ratio, the films that were acid-treated for 1 h showed a higher WCA than those acid-treated for 5 min. The increase in the WCA with treatment time corresponds to the increase in surface roughness.

At pH 2.2, the 15K PAA ratio and acid treatment time had a different effect on the WCA (Fig. 7(b)). When the acid treatment time was 5 min, the WCA decreased from 147° to 115° as the 15K PAA ratio increased from 0 to 100%. In contrast, when the acid treatment time was 1 h, the WCA decreased slightly from 144° to 140° as the 15K PAA ratio increased. At acid treatment of pH 2.2

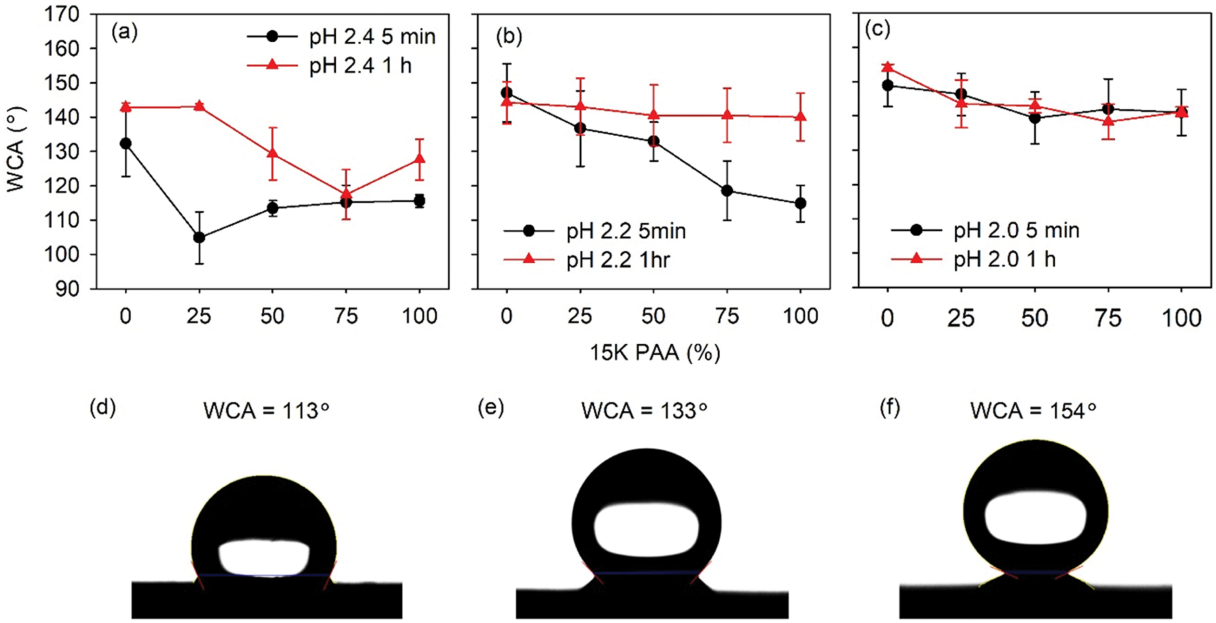


**Fig. 7. WCA of PAH/PAA LbL films with different 15K PAA ratio treated at (a) pH 2.4, (b) pH 2.2, and (c) pH 2.0. Images of water droplets on LbL films assembled and acid-treated at (d) 50% 15K PAA, pH 2.4 for 5 min, (e) 50% 15K PAA, pH 2.2 for 5 min, and (f) 100% 15K PAA, pH 2.0 for 1 h.**

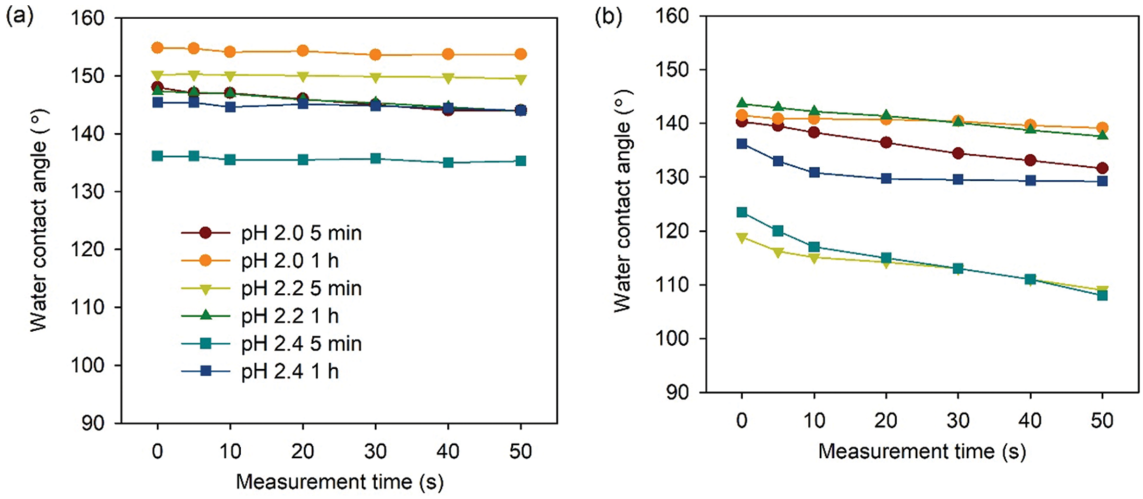


**Fig. 8. Change of WCA with measurement time at varying acid treatment condition for LbL films prepared using 100% of (a) 100K PAA and (b) 15K PAA solution.**

for 1 h, both roughness and pore volume decreased with the increase in 15K PAA ratio. At pH 2.2 for 1 h, roughness of LbL film increased significantly and pore volume decreased as the 15K PAA ratio increased. Therefore, while the WCA decreased 32° at acid treatment time of 5 min due to the decrease in roughness with the increase in 15K PAA ratio, the WCA decreased slightly, around 4°, due to the significant increase in roughness when the films were treated at pH 2.2 for 1 h.

The WCA was also measured for the films treated at pH 2.0 (Fig. 7(c)). One important observation is that the WCA did not decrease substantially as the 15K PAA ratio increased, regardless of the treatment time. The WCA decreased from ~150° to ~140° as the 15K PAA ratio increased. At acid treatment time of 5 min, roughness decreased above 25% of 15K PAA ratio. The surface became relatively smooth without distinct pore structure as confirmed by SEM images. Pore volume also decreased with the increase in 15K PAA. At the treatment time of 1 h, film became smooth with small roughness value with the increase in 15K PAA ratio. However, pore volume increased from 65 to 80% as the 15K PAA ratio increased from 0 to 100%. Thus, decrease in WCA with increasing 15K PAA ratio was significantly suppressed although the roughness decreased for both acid treatment time of 5 min and 1 h. The suppression of decrease in WCA cannot be due to the pore volume effect because pore volume either increased or

decreased depending on acid treatment time. Smooth dense surface over large pore structure seems to inhibit the water penetration or rearrangement of polymer chain on the surface.

To study the effects of 15K PAA ratio and pH on the WCA further, the WCA was measured as a function of time under different acid treatment conditions (Fig. 8). Samples assembled with 100% 100K and 15K PAA were compared. For the films assembled with 100% 100K PAA, the WCA did not change substantially over time, regardless of acid treatment conditions. In contrast, the WCA of the film assembled with 100% 15K PAA was dependent on the pH and treatment time. At pH 2.4 and 2.2 for 5 min, the WCA decreased by 16° and 10°, respectively. At pH 2.2 and pH 2.0 for 1 h, the WCA did not change substantially over time. The WCA decreased by 6° and 2°, respectively.

The decrease in the WCA over time is attributed to partial penetration of water into the film [45,46] or rearrangement of the polymer chain segments on the surface [47,48]. Thus, it can be interpreted that LbL films prepared with 15K PAA facilitate the penetration of water or surface rearrangements compared to those prepared with 100K PAA. However, the decrease in the WCA over time was suppressed as the acid treatment conditions became severe. When the films were treated at pH 2.2 for 1 h, the roughness increased with increasing 15K PAA ratio, which suppressed the decrease of WCA. In contrast, when the films were treated at pH 2.0 for 1 h, the decrease of WCA was suppressed although the films surface was fairly smooth. Smooth dense surface might have interfered the water penetration into the large pores inside the LbL film or hindered polymer chain rearrangement on the surface. Therefore, severe acid treatment played a role to alleviate the decrease of WCA.

## CONCLUSION

This study demonstrates that surface morphology and roughness can be controlled by adjusting the 100K/15K PAA ratio during film assembly and the post assembly acid treatment conditions, pH and time. At an acid treatment time of 5 min, the porous surface structure became smoother as the 15K PAA ratio increased. However, at a treatment time of 1 h, the effect of the 15K PAA ratio on the surface morphologies and surface roughness was influenced by the acid treatment pH. At pH 2.4 and pH 2.0 the roughness decreased as the 15K PAA ratio increased, but the roughness increased significantly at pH 2.2. Furthermore, the relationship between the pore volume and 15K PAA ratio was greatly affected by the pH and treatment time. In particular, at an acid treatment time of 1 h, the pore volume decreased as the 15K PAA ratio increased at pH 2.4, but the pore volume increased as the 15K PAA ratio increased at pH 2.0.

Furthermore, the WCA of porous LbL films treated with TCPFS was affected by the 15K PAA ratio and the pH treatment condition. At pH 2.4, the WCA decreased 15-26° as the 15K PAA ratio increased for acid treatment times of 5 min and 1 h. At pH 2.2, the WCA decreased by 32° as the 15K PAA ratio increased for an acid treatment time of 5 min; however, it only decreased by 4° as the 15K PAA ratio increased when the acid treatment time was 1 h. At pH 2.0, the WCA decreased by approximately 10°, regardless of the acid treatment time. The stability of the WCA over time was affected by the molecular weight of the PAA. The WCA was fairly stable when the films were assembled with 100K PAA. However, when they were assembled with 15K PAA, the stability depended on the acid treatment conditions. At mild acid treatment conditions, the WCA decreased over time and the WCA became stable as the pH decreased and treatment time increased. In summary, it is possible to control the surface morphology of porous LbL films and subsequently the WCA of the fluorinated surface can be managed by adjusting the 100K/15K PAA ratio and the acid treatment conditions.

## ACKNOWLEDGEMENTS

This work was supported by the National Research Foundation of Korea (NRF) grant funded by the Korea government (MSIT) (2018R1C1B5085125). This research was also supported by Basic Science Research Capacity Enhancement Project through Korea Basic Science Institute (Core-facility for Converging Materials) grant funded by the Ministry of Education (2019R1A6C1010045).

## REFERENCES

1. H. Lee, M. L. Alcaraz, M. F. Rubner and R. E. Cohen, *ACS Nano*, **7**, 2172 (2013).
2. Y. Lu, S. Sathasivam, J. L. Song, C. R. Crick, C. J. Carmalt and I. P. Parkin, *Science*, **347**, 1132 (2015).
3. Z. Y. Y. C. Jung and B. Bhushan, *J. Phys.-Condens. Matter*, **22**, 03514 (2010).
4. Z. Y. Deng, W. Wang, L. H. Mao, C. F. Wang and S. Chen, *J. Mater. Chem. A*, **2**, 4178 (2014).
5. T. T. Isimjan, T. Y. Wang and S. Rohani, *Chem. Eng. J.*, **210**, 182 (2012).
6. W. B. Zhang, Y. Z. Zhu, X. Liu, D. Wang, J. Y. Li, L. Jiang and J. Jin, *Angew. Chem., Int. Ed.*, **53**, 856 (2014).
7. B. Su, Y. Tian and L. Jiang, *J. Am. Chem. Soc.*, **138**, 1727 (2016).
8. Z. X. Wang, M. Elimelech and S. H. Lin, *Environ. Sci. Technol.*, **50**, 2132 (2016).
9. Y. F. Si and Z. G. Guo, *Nanoscale*, **7**, 5922 (2015).
10. K. S. Liu, Y. Tian and L. Jiang, *Prog. Mater. Sci.*, **58**, 503 (2013).
11. C. H. Xue, Y. R. Li, P. Zhang, J. Z. Ma and S. T. Jia, *ACS Appl. Mater. Interfaces*, **6**, 10153 (2014).
12. S. L. Zheng, C. Li, Q. T. Fu, W. Hu, T. F. Xiang, Q. Wang, M. P. Du, X. C. Liu and Z. Chen, *Mater. Des.*, **93**, 261 (2016).
13. M. Li, J. Zhai, H. Liu, Y. L. Song, L. Jiang and D. B. Zhu, *J. Phys. Chem. B*, **107**, 9954 (2003).
14. N. J. Shirtcliffe, G. McHale, M. I. Newton and C. C. Perry, *Langmuir*, **19**, 5626 (2003).
15. D. M. Zang, R. W. Zhu, W. Zhang, X. Q. Yu, L. Lin, X. L. Guo, M. J. Liu and L. Jiang, *Adv. Funct. Mater.*, **27**, 1605446 (2017).
16. X. F. Wang, B. Ding, J. Y. Yu and M. R. Wang, *Nano Today*, **6**, 510 (2011).
17. Y. Li, L. Li and J. Q. Sun, *Angew. Chem. Int. Ed.*, **49**, 6129 (2010).
18. X. Du, X. M. Liu, H. M. Chen and J. H. He, *J. Phy. Chem. C*, **113**, 9063 (2009).
19. P. S. Brown and B. Bhushan, *Sci. Rep.*, **5**, 8701 (2015).

20. X. Y. Huang, J. D. Chrisman and N. S. Zacharia, *ACS Macro Lett.*, **2**, 826 (2013).
21. X. Y. Huang and N. S. Zacharia, *J. Appl. Poly. Sci.*, **132**, 42767 (2015).
22. T. Soeno, K. Inokuchi and S. Shiratori, *Appl. Surf. Sci.*, **237**, 543 (2004).
23. X. J. Guo, C. H. Xue, M. Li, X. Li and J. Z. Ma, *RSC Adv.*, **7**, 25560 (2017).
24. S. Hwangbo, J. Heo, X. Lin, M. Choi and J. Hong, *Sci. Rep.*, **6**, 19178 (2016).
25. L. Zhang and J. Q. Sun, *Macromolecules*, **43**, 2413 (2010).
26. M. C. Wu, N. An, Y. Li and J. Q. Sun, *Langmuir*, **32**, 12361 (2016).
27. J. Ji, J. H. Fu and J. C. Shen, *Adv. Mater.*, **18**, 1441 (2006).
28. J. H. Fu, J. Ji, L. Y. Shen, A. Kueller, A. Rosenhahn, J. C. Shen and M. Grunze, *Langmuir*, **25**, 672 (2009).
29. X. K. Liu, B. Y. Dai, L. Zhou and J. Q. Sun, *J. Mater. Chem.*, **19**, 497 (2009).
30. M. E. Buck, S. C. Schwartz and D. M. Lynn, *Chem. Mater.*, **22**, 6319 (2010).
31. U. Manna, A. H. Broderick and D. M. Lynn, *Adv. Mater.*, **24**, 4291 (2012).
32. J. D. Mendelsohn, C. J. Barrett, V. V. Chan, A. J. Pal, A. M. Mayes and M. F. Rubner, *Langmuir*, **16**, 5017 (2000).
33. J. Hiller, J. D. Mendelsohn and M. F. Rubner, *Nat. Mater.*, **1**, 59 (2002).
34. C. Sung, Y. Ye and J. L. Lutkenhaus, *ACS Macro Lett.*, **4**, 353 (2015).
35. J. L. Lutkenhaus, K. McEnnis and P. T. Hammond, *Macromolecules*, **41**, 6047 (2008).
36. C. Cho and N. S. Zacharia, *Langmuir*, **28**, 841 (2012).
37. K.-K. Chia, M. F. Rubner and R. E. Cohen, *Langmuir*, **25**, 14044 (2009).
38. L. Zhai, F. Ç. Cebeci, R. E. Cohen and M. F. Rubner, *Nano Lett.*, **4**, 1349 (2004).
39. J. Yu, S. Han, J. S. Hong, O. Sanyal and I. Lee, *Langmuir*, **32**, 8494 (2016).
40. B. Sun, R. M. Flessner, E. M. Saurer, C. M. Jewell, N. J. Fredin and D. M. Lynn, *J. Colloid Interface Sci.*, **355**, 431 (2011).
41. X. Chen and J. Sun, *Chem.- Asian J.*, **9**, 2063 (2014).
42. P. S. Brown and B. Bhushan, *J. Colloid Interface Sci.*, **456**, 210 (2015).
43. P. S. Brown and B. Bhushan, *Sci. Rep.*, **5**, 14030 (2015).
44. J. Yu, B. M. Meharg and I. Lee, *Polymer*, **109**, 297 (2017).
45. Y. Wang, J. Knapp, A. Legere, J. Raney and L. Li, *RSC Adv.*, **5**, 30570 (2015).
46. H. Choi and H. Liang, *J. Colloid Interface Sci.*, **477**, 176 (2016).
47. H. Sawada, Y. Ikematsu, T. Kawase and Y. Hayakawa, *Langmuir*, **12**, 3529 (1996).
48. A. Vaidya and M. K. Chaudhury, *J. Colloid Interface Sci.*, **249**, 235 (2002).